Letter | Editors' Suggestion

Quantum geometric origin of the intrinsic nonlinear Hall effect

Yannis Ulrich [1,2,*] Johannes Mitscherling [3] Laura Classen [1,2] and Andreas P. Schnyder [1]

[1] *Max Planck Institute for Solid State Research, D-70569 Stuttgart, Germany*

[2] *School of Natural Sciences, Technische Universität München, D-85748 Garching, Germany*

[3] *Max Planck Institute for the Physics of Complex Systems, Nöthnitzer Strasse 38, D-01187 Dresden, Germany*

(Received 7 July 2025; accepted 10 April 2026; published 4 May 2026)

We decompose the intrinsic second-order nonlinear Hall effect (NLHE) of a generic multiband system into its quantum geometric contributions within a fully quantum-mechanical, projector-based formalism. By expanding the nonlinear conductivity in powers of the quasiparticle lifetime τ, we recover the established Berry curvature dipole at order τ and clarify discrepancies in previous literature concerning the (interband) quantum metric dipole (or Berry curvature polarizability) contribution at order τ^0. Crucially, our method reveals an additional contribution at order τ^0, determined by the *intraband* quantum metric dipole (intraQMD), arising from additional virtual interband transitions captured within the fully quantum-mechanical treatment. The intraQMD contribution is generically nonzero in systems with broken time-reversal symmetry and can be distinguished from other geometric contributions by symmetry. Analytical results for low-energy models of topological band crossings, which are hot spots of quantum geometry, demonstrate how band topology influences each contribution. In particular, the intraQMD contribution is especially large in gapped Dirac cones in antiferromagnets. Through a comprehensive symmetry classification of all magnetic space groups, we identify several candidate materials that are expected to exhibit large intrinsic NLHE, including the topological antiferromagnets Yb_3Pt_4, CuMnAs, and $CoNb_3S_6$, as well as the nodal-plane material $MnNb_3S_6$.

DOI: 10.1103/4z8z-4kch

Introduction. Quantum geometry, such as the Berry curvature and the quantum metric, has become an essential tool for understanding wave-function properties of materials and relating them to physical responses [1–4]. While the Berry curvature, whose integral is the Chern number, describes intrinsic linear Hall effects, the quantum metric is intimately connected to nonlinear responses, such as second-harmonic generation, bulk photovoltaic effects, and the nonlinear Hall effect [5–39]. In strongly correlated systems, on the other hand, quantum geometry can guarantee finite superfluidity [40] and stabilize fractional Chern insulators [41].

The anomalous Hall effect establishes a direct connection between band topology and Berry curvature, being proportional to the integral of the latter over the Brillouin zone. In topological materials, concentrated Berry curvature originating from (near) band degeneracies, such as Weyl nodes or nodal planes, can strongly enhance the response [42–47].

In contrast, this connection is less understood in the nonlinear regime, where additional virtual interband transitions relate to state properties that are captured by more diverse quantum geometric invariants than just the Berry curvature [6,32,34,48–52]. These invariants are also generically large near (gapped) topological band crossings, and extend to regimes where conventional contributions are symmetry forbidden or strongly suppressed. For example, in time-reversal symmetric systems, where the linear anomalous Hall response vanishes, the Berry curvature dipole yields a lifetime-dependent nonlinear Hall contribution [53].

However, the systematic investigation of nonlinear responses in terms of distinct quantum geometric invariants remains challenging. In particular, the lifetime-independent contribution, attributed to the interband quantum metric dipole (or Berry curvature polarizability), has been debated, with different semiclassical approaches leading to conflicting predictions [31,33,54,55]. This ambiguity is particularly consequential in $\mathcal{PT}$-symmetric antiferromagnets, where lifetime-independent terms are expected to dominate, and has already led to contradictory experimental interpretations [37,56].

In this Letter, we present a comprehensive, fully gauge-invariant projector-based Green's-function framework that systematically decomposes the second-order nonlinear Hall effect (NLHE) into its quantum geometric contributions [6,51,57–63]. Our approach recovers the Berry curvature dipole and the interband quantum metric dipole (interQMD), confirmed by the results of a very recent reassessment [64] of deviating semiclassical results [31,33,54,55], and reveals a third lifetime-independent contribution originating from the momentum derivative of the intraband quantum metric (intraQMD). This framework applies to both nondegenerate and degenerate bands, enabling analytical, gauge-invariant expressions for representative (gapped) Dirac/Weyl points, nodal lines, and nodal planes that serve as minimal models for the

*Contact author: y.ulrich@fkf.mpg.de

Published by the American Physical Society under the terms of the Creative Commons Attribution 4.0 International license. Further distribution of this work must maintain attribution to the author(s) and the published article's title, journal citation, and DOI. Open access publication funded by Max Planck Society.

different contributions. By combining the analytical results with a comprehensive symmetry analysis for all magnetic space groups (MSGs), we obtain stringent search and design criteria for materials with large intrinsic NLHE, as required for high-frequency rectifiers and spintronic memory devices [65–67]. The presented framework sets the stage for a systematic exploration of other nonlinear DC responses, advancing the ongoing research on nonlinear optical responses.

Quantum geometric expansion of the NLHE. We start by calculating the second-order DC conductivity tensor, relating the nonlinear response of the current density to the electric fields via $j^a = \sum_{b,c} \sigma^{a;bc} E^b E^c$, with spatial indices a, b, c, for a general quadratic Hamiltonian

$$\hat{H} = \sum_{\alpha,\beta} \hat{c}^\dagger_\alpha(\mathbf{k}) H_{\alpha\beta}(\mathbf{k}) \hat{c}_\beta(\mathbf{k}). \tag{1}$$

The Hamiltonian defines the Bloch Hamiltonian matrix $\hat{H}(\mathbf{k}) = [H_{\alpha\beta}(\mathbf{k})]$ given in the "orbital" basis, which may include spin, atomic orbitals, sublattice, or other degrees of freedom within the unit cell, with corresponding creation operators for fixed lattice momentum denoted by $\hat{c}^\dagger_\alpha(\mathbf{k})$. Using Green's-function formalism, the nonlinear DC conductivity is given by [68–70]

$$\begin{aligned}\sigma^{a;bc} = -\frac{e^3}{\hbar} \int_{\mathrm{BZ}} \frac{d^d\mathbf{k}}{(2\pi)^d} \int_{-\infty}^{\infty} d\epsilon \frac{\partial f(\epsilon)}{\partial \epsilon} \\ \times \mathrm{Re}\,\mathrm{tr}\Bigg[\hat{A}(\epsilon,\mathbf{k}) \hat{H}^a(\mathbf{k}) \frac{\partial \hat{G}^R(\epsilon,\mathbf{k})}{\partial \epsilon} \\ \times \left(\hat{H}^b(\mathbf{k}) \hat{G}^R(\epsilon,\mathbf{k}) \hat{H}^c(\mathbf{k}) + \frac{1}{2} \hat{H}^{bc}(\mathbf{k}) + (b \leftrightarrow c) \right) \Bigg],\end{aligned} \tag{2}$$

involving momentum derivatives $\hat{H}^a(\mathbf{k}) = \partial_{k_a} \hat{H}(\mathbf{k})$ and $\hat{H}^{ab}(\mathbf{k}) = \partial_{k_a} \partial_{k_b} \hat{H}(\mathbf{k})$ of the Bloch Hamiltonian, the retarded Green's function $\hat{G}^R(\epsilon,\mathbf{k}) = [\epsilon + \mu - \hat{H}(\mathbf{k}) + i\Gamma]^{-1}$ with chemical potential μ, the Fermi-function distribution $f(\epsilon)$ at temperature $k_B T$, and the spectral function $\hat{A}(\epsilon,\mathbf{k}) = -\pi\, \mathrm{Im}\, \hat{G}^R(\epsilon,\mathbf{k})$. We introduce a phenomenological constant and nonzero imaginary part of the electron self-energy $\Gamma > 0$ [71–76], capturing the electron lifetime $\tau = 1/2\Gamma$. It corresponds to a broadening of the spectral density and can, e.g., be derived microscopically from white-noise disorder within a self-consistent Born approximation [77,78]. A finite-electron lifetime is required to regularize the conductivity in the DC limit. Further discussion of this approximation and a generalization to a band-dependent self-energy is provided in the Supplemental Material (SM) [68].

The matrices within the trace in Eq. (2) generally do not commute, reflecting the nontrivial multiband nature of the system, which we characterize in terms of quantum geometry. In the following, we focus on $\sigma^{a;bb}$, which is most relevant for experiments, while the more general case $b \neq c$ is treated in the SM [68]. To reveal the relevant quantum geometric invariants for $\sigma^{a;bb}$, we diagonalize the Bloch Hamiltonian matrix, yielding

$$\hat{H}(\mathbf{k}) = \sum_{n \in \mathrm{bands}} E_n(\mathbf{k}) \hat{P}_n(\mathbf{k}), \tag{3}$$

with dispersion $E_n(\mathbf{k})$ and orthogonal projector $\hat{P}_n(\mathbf{k})$ onto the (non)degenerate bands.

Importantly, all subsequent quantities, expressed in projectors, are manifestly gauge invariant. The nontrivial geometry arises from virtual interband transitions due to the coupling to the electric field and can be systematically characterized through a "quantum geometric expansion" of $\sigma^{a;bb}$ obtained by inserting Eq. (3) into Eq. (2). In this expansion, we separate band-dependent quantities, such as the direct band gap $\epsilon_{mn} = E_m - E_n$, the quasiparticle velocity $v^a_n = \partial_{k_a} E_n$, and the quasiparticle mass $m^{ab}_n = (\partial_{k_a} \partial_{k_b} E_n)^{-1}$, from quantum geometric invariants expressed as traces over projectors $\hat{P}_n$ and their derivatives $\partial_{k_a} \hat{P}_n$ [51,63].

In order to determine the leading-order contributions to the nonlinear DC response systematically, we combine the quantum geometric expansion with a perturbative expansion in $1/(\tau W)$ with bandwidth W and keep the three dominant orders τ^2, τ^1, and τ^0. The straightforward but technical steps of the derivation are provided in the Supplemental Material [68]. In the zero-temperature limit, this yields the leading-order decomposition

$$\begin{aligned}\sigma^{a;bb} = \frac{e^3}{\hbar} \sum_{n \in \mathrm{bands}} \int \frac{d^d\mathbf{k}}{(2\pi)^d} \delta(E_n(\mathbf{k}) - \mu) \big[\sigma^{a;bb}_{\mathrm{NLD}}(\mathbf{k}) \\ + \sigma^{a;bb}_{\mathrm{BCD}}(\mathbf{k}) + \sigma^{a;bb}_{\mathrm{interQMD}}(\mathbf{k}) + \sigma^{a;bb}_{\mathrm{intraQMD}}(\mathbf{k}) \big],\end{aligned} \tag{4}$$

for which we summarize the four distinct contributions, their scaling in the quasiparticle lifetime τ, and the relevant quantum geometric quantities in the manifestly gauge-invariant projector form in Table I. These results can be extended to finite temperature. We identify four relevant quantum geometric invariants for the NLHE that cannot be further reduced up to partial integration in momentum: the band degeneracy N_n, Berry curvature Ω^{ab}_n, two-state quantum metric g^{ab}_{mn}, and quantum metric dipole $\partial_{k_a} g^{bb}_n$. We fixed the ambiguity arising from partial integration in momentum by providing all expressions as Fermi-surface contributions.

Distinct quantum geometric origins of the NLHE. The nonlinear Drude weight (NLD), or Drude weight dipole, arises at order τ^2 and only trivially depends on the quantum states via the band degeneracy $N_n = \mathrm{tr}[\hat{P}_n]$ [79,80]. We find a further contribution proportional to N_n at subleading order τ^0 given by $\int_{\mathbf{k}} \sum_n \frac{1}{24} \delta'(E_n) \frac{v^a_n(\mathbf{k})}{m^{bb}_n(\mathbf{k})} N_n(\mathbf{k})$, as shown in the SM [68]. The remaining three contributions are due to virtual interband transitions conveniently captured by the product of gauge-invariant interband transition operators $\hat{e}^a_{nm} = i \hat{P}_n \partial_{k_a} \hat{P}_m \hat{P}_m$ [6,48,51]. We employ the defining properties of orthogonal projectors $\sum_n P_n = \mathbb{1}$ and $P_m P_n = \delta_{mn} P_m$ to systematically simplify the expressions by identifying the relevant quantum geometric invariants; see Table I [51,68]. At order τ^1, we recover the well-established Berry curvature dipole (BCD) [53].

At order τ^0, we find two distinct contributions. The first one involves the two-state quantum metric g^{ab}_{mn}, and is commonly referred to as the (interband) quantum metric dipole (interQMD) [54]. While alternative approaches, such as the Luttinger-Kohn method [33], a Moyal product expansion [81], or other semiclassical treatments [31,55,82], yield qualitatively similar terms, they differ in coefficients and symmetry

TABLE I. Full expressions for the leading-order contributions of distinct quantum geometric origin to the nonlinear conductivity, Eq. (4), together with their scaling in the quasiparticle lifetime τ. The explicitly appearing quantum geometric invariants are the band degeneracy $N_n(\mathbf{k})$, Berry curvature $\Omega_n^{ab}(\mathbf{k})$, quantum metric $g_{mn}^{ab}(\mathbf{k})$, and quantum metric dipole $\partial_{k_a} g_n^{bb}(\mathbf{k})$. Symmetry conditions for all components of Eq. (4) are shown for the representative case $\sigma^{x;yy}$. A check mark (✓) indicates that a term is allowed under the corresponding symmetry. A complete table of nonzero tensor components, together with a magnetic space group analysis, is provided in the Supplemental Material [68]. $\mathcal{P}$, $\mathcal{T}$, $\mathcal{C}_n$, and $\mathcal{M}$ denote inversion, time-reversal, n-fold rotation, and mirror symmetries, respectively.

	Nonlinear Drud weight (NLD)	Berry curvature dipole (BCD)	Interband quantum metric dipole(interQMD)	Intraband quantum metric dipole(intraQMD)
Symbol	$\sigma^{a;bb}_{\mathrm{NLD}}(\mathbf{k})$	$\sigma^{a;bb}_{\mathrm{BCD}}(\mathbf{k})$	$\sigma^{a;bb}_{\mathrm{interQMD}}(\mathbf{k})$	$\sigma^{a;bb}_{\mathrm{intraQMD}}(\mathbf{k})$
Full expression	$-\tau^2 \frac{v_n^a(\mathbf{k})}{m_n^{bb}(\mathbf{k})} N_n(\mathbf{k})$	$\tau\, v_n^b(\mathbf{k}) \Omega_n^{ab}(\mathbf{k})$	$\sum_{m\neq n} 2 \frac{v_n^b(\mathbf{k}) g_{mn}^{ab}(\mathbf{k}) - v_n^a(\mathbf{k}) g_{mn}^{bb}(\mathbf{k})}{\epsilon_{mn}(\mathbf{k})}$	$-\frac{1}{2} \partial_{k_a} g_n^{bb}(\mathbf{k})$
Lifetime scaling	τ^2	τ	τ^0	τ^0
Quantum geometric invariant	$N_n(\mathbf{k})$	$\Omega_n^{ab}(\mathbf{k})$	$g_{mn}^{ab}(\mathbf{k})$	$\partial_{k_a} g_n^{bb}(\mathbf{k})$
	$\mathrm{tr}[\hat{P}_n]$	$i\,\mathrm{tr}[\hat{P}_n\,[\partial_{k_a}\hat{P}_n,\ \partial_{k_b}\hat{P}_n]]$	$\frac{1}{2}\mathrm{tr}[\partial_{k_a}\hat{P}_m\,\partial_{k_b}\hat{P}_n]$	$\mathrm{tr}[\partial_{k_a}\partial_{k_b}\hat{P}_n\,\partial_{k_a}\hat{P}_n]$
$\mathcal{P}$	✗	✗	✗	✗
$\mathcal{T}$	✗	✓	✗	✗
$\mathcal{PT}$	✓	✗	✓	✓
$C_2^z,\ C_2^x,\ \mathcal{M}_x$	✗	✗	✗	✗
$C_2^y,\ \mathcal{M}_y$	✓	✓	✓	✓
C_3^z	✓	✗	✗	✓

behavior, particularly in $\mathcal{C}_3$-symmetric systems [33,54]. These inconsistencies have led to conflicting interpretations of experiments [37,56]. Our formulation, based solely on the Green's-function expression Eq. (2) and a constant imaginary self-energy, agrees with the result of Gao *et al.* [54], and is consistent with the recent independent reinvestigation of the semiclassical theories [64].

The second contribution at order τ^0 involves the dipole of the *intraband quantum metric* $\partial_{k_a} g_n^{bb}$, which we label as the intraband quantum metric dipole (intraQMD). It has not yet been identified in any aforementioned calculations [31,33,54,81] to the best of our knowledge. The quantum metric dipole arises from symmetrized and band-traced two-state quantum geometric connections $\mathrm{tr}[\hat{e}^b_{nm}\partial_{k_a}\hat{e}^c_{mn}]$ and three-band contributions $\mathrm{tr}[\hat{e}^a_{nm}\hat{e}^b_{ml}\hat{e}^c_{ln}]$ [51,68,83], showing its nontrivial interband origin. These contributions are present in Feynman diagrams containing only off-diagonal photon vertices, which distinguishes them from processes arising from extrinsic mechanisms such as skew scattering or side jumps [69]. It originates from virtual interband processes captured naturally in the Green's-function formalism but absent in semiclassical approaches, where quasiparticles are assigned delta-function spectral weight and lifetime effects enter only through a relaxation-time approximation [84]. We discuss the difference to semiclassical methods further in the SM [68]. Note that the coefficient of the intraQMD is independent of the band structure.

Numerically, the separation of quantum geometry and band structure enables efficient evaluation in many cases [57,85]. Besides the numerical differentiation schemes based on finite differences, derivatives of the projectors can be replaced by appropriate combinations of derivatives of the Bloch Hamiltonian matrix [68].

Distinguishing contributions by symmetries. In the linear case, dissipative and nondissipative (Hall) components correspond to the symmetric and antisymmetric parts of the conductivity tensor σ^{ab} with $j^a = \sigma^{ab}E^b$. In the nonlinear case, this separation is more subtle and requires the full tensor $\sigma^{a;bc}$. Details are given in the SM [68]; importantly, all components of $\sigma^{a;bc}$ can be accessed experimentally [86].

The different contributions can be distinguished by their transformation properties under common symmetries [33,68,87,88], as summarized in Table I. In the SM [68], we provide the list of nonzero tensor components for each contribution. In particular, for antiferromagnetic order with the magnetic $\mathcal{PT}$ symmetry, all terms except the BCD contribute. Moreover, $\mathcal{C}_3$ symmetry forbids the BCD and interQMD contributions, leaving the intraQMD as the only geometric response. Below, we will extend this magnetic symmetry analysis to identify material candidates.

To quantify the relevance of the different contributions beyond the symmetry analysis and establish their connection to band topology, we derive analytical results for the NLHE in several representative low-energy models. We focus on noncentrosymmetric systems with broken time-reversal symmetry, thereby allowing for contributions beyond the BCD (see Table I). The zero-, one-, or two-dimensional degeneracies in momentum space can be locally approximated by low-energy Hamiltonians. In the following, we discuss a $\mathcal{PT}$-symmetric 3D tilted Dirac point. In the SM [68], we provide results for the two-dimensional (2D) tilted Dirac point, a 3D nodal line, and a 3D nodal plane, along with a description of the analytic methods employed. An overview of the discussed models is provided in Table II.

3D tilted Dirac point. To elucidate the behavior of QMD-driven contributions (inter- and intraQMD), we begin by investigating a four-band $\mathcal{PT}$-symmetric 3D tilted Dirac point with uniform velocity v described by the Hamiltonian

$$H = tk_y\sigma_0\tau_0 + v(k_x\sigma_z\tau_x + k_y\sigma_0\tau_y + k_z\sigma_x\tau_x) + m\sigma_y\tau_x, \quad (5)$$

with the tensor product of Pauli matrices τ and σ. Antiferromagnetic systems with $\mathcal{PT}$ symmetry have recently been studied to identify contributions to the NLHE beyond the BCD [56,89,90]. A mass term proportional to m is introduced,

TABLE II. Contributions found for the minimal (tilted) Weyl/Dirac, nodal line, and nodal plane models discussed in the main text and the SM [68]. Here, minimal indicates that terms of higher order in k are neglected, which are typically much smaller than the leading ones.

	NLD	BCD	interQMD	intraQMD
Gapped Dirac point in 3D	✓	✗	✓	✓
Gapless Weyl point in 3D	✓	✗	✓	✗
Gapped Dirac point in 2D	✓	✓	✓	✓
Gapless Dirac point in 2D	✓	✗	✓	✓
Nodal line in 3D	✓	✓	✓	✓
Nodal plane in 3D	✓	✗	✓	✓

which breaks $\mathcal{P}$ and $\mathcal{T}$ individually, while preserving $\mathcal{PT}$. The tilt parameter $t \propto \mathbb{1}$ also breaks inversion symmetry, affecting the Fermi surface but not the quantum geometry. Thus, to obtain contributions to the NLHE, we effectively compute skewed averages of the underlying quantum geometry of a Dirac point. This is illustrated in Figs. 1(a) and 1(b), where we plot the inter- and intraQMD contributions prior to integration in a cross section of $\mathbf{k}$ space, along with the skewed Fermi surfaces. The model also possesses mirror symmetries $\mathcal{M}_x$, $\mathcal{M}_z$, which, as indicated in Table I, imply that the only nonzero Hall conductivities are $\sigma^{y;xx} = \sigma^{y;zz}$. $\mathcal{PT}$ symmetry enforces that the BCD contribution vanishes. The material CuMnAs realizes such Dirac points near the Fermi energy and has previously been connected to the NLHE [89,91]. Under pressure, Bi_2CuO_4 may also exhibit Dirac points near the Fermi surface in an antiferromagnetic phase [92].

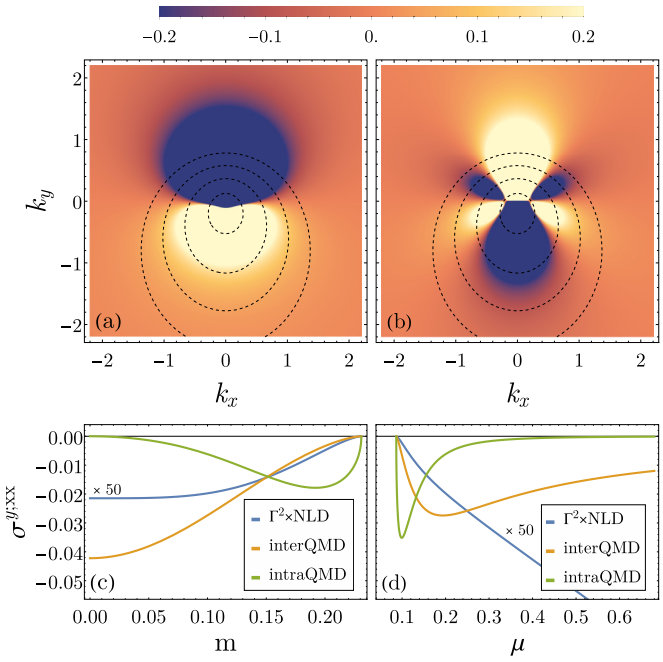


FIG. 1. The (a) inter- and (b) intraQMD contributions before $\mathbf{k}$ integration along the cut of momentum space $k_z = 0$ for the 3D Dirac model defined in Eq. (5) with velocity $v = 1$, tilt $t = 0.5$, and mass $m = 0.2$. We give the dependence of the three nonzero contributions on (c) the gap m for $\mu = 0.2$ and (d) the chemical potential μ for $m = 0.1$ of $\sigma^{y;xx}$. In both cases, the chemical potential lies within the upper band.

Note that the model consists of two doubly degenerate bands. The projector formalism is particularly convenient in this case, as it effectively reduces the system to a two-band model with projectors $\hat{P}_1(\mathbf{k})$ and $\hat{P}_2(\mathbf{k})$ projecting onto the entire degenerate eigenspaces of each band. Analytic expressions for the conductivities are obtained and presented in the SM [68]. All contributions except for the BCD are nonzero. The results are plotted in Figs. 1(c) and 1(d) as functions of m and μ. At a fixed chemical potential $\mu = 0.2$, the intraQMD contribution dominates for larger gap sizes. For a fixed gap $m = 0.1$, the intraQMD and interQMD contributions are of equal importance when approaching the band edge. Particle-hole symmetry enforces that all contributions are odd functions of μ [68], which is confirmed by the analytic expressions. When the mass m is set to 0, the Hamiltonian can be block-diagonalized into two gapless 3D Weyl points, with nonzero NLD and interQMD contributions. The latter is proportional to $1/\mu$, diverging at the band crossing point [68].

Extending the analysis to 3D nodal lines and planes completes the treatment of zero-, one-, and two-dimensional band degeneracies. For both the nodal line and plane, contributions increase as the band feature is made flatter, which can be understood in terms of an increased density of states. While for nodal lines QMD-driven contributions are strongly enhanced for a vanishing mass gap, the intraQMD is found to be proportional to the gap in the minimal nodal-plane model [68,93].

Candidate materials. To identify materials exhibiting an NLHE driven by quantum geometric invariants beyond the BCD, we derive symmetry constraints for all magnetic space groups (MSGs), resulting in four distinct scenarios, each associated with candidate materials drawn from MAGNDATA [94,95]. Complete MSG listings and additional candidates are provided in the SM [68]. Representative examples include Yb_3Pt_4, which realizes a case where, within a given plane, the BCD and interQMD are forbidden while the intraQMD remains symmetry allowed. Another example is $MnNb_3S_6$, a metallic ferromagnetic system with nodal-plane-enhanced quantum geometry, in which the BCD is forbidden, but both interQMD and intraQMD are allowed.

Discussion. Within a fully gauge-invariant approach, we identified three quantum geometric contributions to the second-order nonlinear Hall effect, including a previously unrecognized intraband quantum metric dipole (intraQMD). Our approach reproduces the established semiclassical contributions (NLD and BCD) while resolving prior discrepancies surrounding the interband quantum metric dipole (interQMD). A magnetic symmetry analysis revealed nodal-plane materials and antiferromagnetic Dirac systems as promising candidates for quantum-metric-dipole-driven NLHE, complementing the Berry-curvature-driven response.

Disorder and interactions are expected to generate additional quantum geometric structure in nonlinear Hall responses. Our quantum geometric Green's-function expansion provides a framework to incorporate microscopic scattering and assess whether further invariants emerge. Temperature-dependent measurements may distinguish contributions through their characteristic scattering-rate scaling,

including the nonlinear Drude and quantum metric dipole terms or other extrinsic effects [36,37].

An even richer dependence on quantum geometric invariants beyond the quantum metric and Berry curvature can be expected for disorder- and interaction-induced nonlinear Hall responses when combining microscopic impurity or electron-phonon scattering with nontrivial Bloch states. While numerical progress has been made for minimal models, such as the 2D Dirac point [69], a complete understanding remains an open challenge. The presented quantum geometric expansion provides a suitable framework, starting from a perturbative Green's function approach, to enable studies of how contributions are modified and whether additional geometric invariants emerge. Temperature-dependent experiments may help separate contributions via the distinct scaling in the scattering rate, such as the nonlinear Drude and quantum metric dipole contributions, or new extrinsic effects [36,37].

The presented techniques can also be straightforwardly extended to further DC responses, such as the spin Hall, Nernst, and DC Kerr effects in the nonlinear regime. Additionally, our scattering rate expansion [68] also enables access to higher-order effects such as third-order or magnetononlinear Hall responses [54]. A systematic understanding of the quantum geometric structure of nonlinear responses may reveal unexpected links between observables, clarify the role of emerging geometric invariants [6,32,34,48–51,61,63], and guide the design of nonlinear phenomena in quantum materials.

Note added. Recently, we became aware of a related work [96], in which the nonlinear conductivity was calculated using the density-matrix formalism for a system coupled to a featureless bath and subsequently decomposed into its quantum geometric contributions. Their five contributions are fully consistent with ours.

Acknowledgments. We thank Pavel Ostrovsky for deriving Eq. (2) and for enlightening us about the role of disorder on the NLHE. The authors are also grateful to Tobias Holder, Moritz Hirschmann, and Raymond Wiedmann for helpful discussions. Y.U., L.C., and A.P.S. are funded by the Deutsche Forschungsgemeinschaft (DFG, German Research Foundation)–TRR 360-492547816. J.M. was, in part, supported by the Deutsche Forschungsgemeinschaft under Grant cluster of excellence ct.qmat (EXC 2147, Project No. 390858490).

Data availability. The data presented in this manuscript consist of numerical evaluations of the analytic expressions provided in the manuscript and Supplemental Material.

[1] P. Törmä, Essay: Where can quantum geometry lead us? Phys. Rev. Lett. **131**, 240001 (2023).

[2] J. Yu, B. A. Bernevig, R. Queiroz, E. Rossi, P. Törmä, and B.-J. Yang, Quantum geometry in quantum materials, npj Quantum Mater. **10**, 101 (2025).

[3] Y. Jiang, T. Holder, and B. Yan, Revealing quantum geometry in nonlinear quantum materials, Rep. Prog. Phys. **88**, 076502 (2025).

[4] N. Verma, P. J. W. Moll, T. Holder, and R. Queiroz, Quantum geometry: Revisiting electronic scales in quantum matter, Nat. Rev. Phys. **8**, 226 (2026).

[5] T. Holder, D. Kaplan, and B. Yan, Consequences of time-reversal-symmetry breaking in the light-matter interaction: Berry curvature, quantum metric, and diabatic motion, Phys. Rev. Res. **2**, 033100 (2020).

[6] A. Avdoshkin, J. Mitscherling, and J. E. Moore, Multistate geometry of shift current and polarization, Phys. Rev. Lett. **135**, 066901 (2025).

[7] J. Ahn, G.-Y. Guo, and N. Nagaosa, Low-frequency divergence and quantum geometry of the bulk photovoltaic effect in topological semimetals, Phys. Rev. X **10**, 041041 (2020).

[8] P. Zhu and A. Alexandradinata, Anomalous shift and optical vorticity in the steady photovoltaic current, Phys. Rev. B **110**, 115108 (2024).

[9] P. Bhalla, K. Das, D. Culcer, and A. Agarwal, Resonant second-harmonic generation as a probe of quantum geometry, Phys. Rev. Lett. **129**, 227401 (2022).

[10] L. Wu, S. Patankar, T. Morimoto, N. L. Nair, E. Thewalt, A. Little, J. G. Analytis, J. E. Moore, and J. Orenstein, Giant anisotropic nonlinear optical response in transition metal monopnictide Weyl semimetals, Nat. Phys. **13**, 350 (2017).

[11] A. M. Cook, B. M. Fregoso, F. de Juan, S. Coh, and J. E. Moore, Design principles for shift current photovoltaics, Nat. Commun. **8**, 14176 (2017).

[12] F. de Juan, A. G. Grushin, T. Morimoto, and J. E. Moore, Quantized circular photogalvanic effect in Weyl semimetals, Nat. Commun. **8**, 15995 (2017).

[13] J. E. Sipe and A. I. Shkrebtii, Second-order optical response in semiconductors, Phys. Rev. B **61**, 5337 (2000).

[14] Y. Zhang, J. van den Brink, C. Felser, and B. Yan, Electrically tuneable nonlinear anomalous Hall effect in two-dimensional transition-metal dichalcogenides WTe_2 and $MoTe_2$, 2D Mater. **5**, 044001 (2018).

[15] T. Low, Y. Jiang, and F. Guinea, Topological currents in black phosphorus with broken inversion symmetry, Phys. Rev. B **92**, 235447 (2015).

[16] Q. Ma, S.-Y. Xu, H. Shen, D. MacNeill, V. Fatemi, T.-R. Chang, A. M. Mier Valdivia, S. Wu, Z. Du, C.-H. Hsu, S. Fang, Q. D. Gibson, K. Watanabe, T. Taniguchi, R. J. Cava, E. Kaxiras, H.-Z. Lu, H. Lin, L. Fu, N. Gedik, *et al.*, Observation of the nonlinear Hall effect under time-reversal-symmetric conditions, Nature (London) **565**, 337 (2019).

[17] J. I. Facio, D. Efremov, K. Koepernik, J.-S. You, I. Sodemann, and J. van den Brink, Strongly enhanced berry dipole at topological phase transitions in BiTeI, Phys. Rev. Lett. **121**, 246403 (2018).

[18] O. O. Shvetsov, V. D. Esin, A. V. Timonina, N. N. Kolesnikov, and E. V. Deviatov, Nonlinear Hall effect in three-dimensional weyl and Dirac semimetals, JETP Lett. **109**, 715 (2019).

[19] S. Dzsaber, X. Yan, M. Taupin, G. Eguchi, A. Prokofiev, T. Shiroka, P. Blaha, O. Rubel, S. E. Grefe, H.-H. Lai, Q. Si, and S. Paschen, Giant spontaneous Hall effect in a nonmagnetic Weyl–Kondo semimetal, Proc. Natl. Acad. Sci. U.S.A. **118**, e2013386118 (2021).

[20] D. Kumar, C.-H. Hsu, R. Sharma, T.-R. Chang, P. Yu, J. Wang, G. Eda, G. Liang, and H. Yang, Room-temperature nonlinear Hall effect and wireless radiofrequency rectification in Weyl semimetal $TaIrTe_4$, Nat. Nanotechnol. **16**, 421 (2021).

[21] S. Singh, J. Kim, K. M. Rabe, and D. Vanderbilt, Engineering Weyl phases and nonlinear Hall effects in T_d-$MoTe_2$, Phys. Rev. Lett. **125**, 046402 (2020).
[22] C. Zeng, S. Nandy, and S. Tewari, Nonlinear transport in Weyl semimetals induced by Berry curvature dipole, Phys. Rev. B **103**, 245119 (2021).
[23] Z. Z. Du, C. M. Wang, H.-Z. Lu, and X. C. Xie, Band signatures for strong nonlinear Hall effect in Bilayer WTe_2, Phys. Rev. Lett. **121**, 266601 (2018).
[24] J.-S. You, S. Fang, S.-Y. Xu, E. Kaxiras, and T. Low, Berry curvature dipole current in the transition metal dichalcogenides family, Phys. Rev. B **98**, 121109(R) (2018).
[25] C. Xiao, Z. Z. Du, and Q. Niu, Theory of nonlinear Hall effects: Modified semiclassics from quantum kinetics, Phys. Rev. B **100**, 165422 (2019).
[26] J. Son, K.-H. Kim, Y. H. Ahn, H.-W. Lee, and J. Lee, Strain engineering of the berry curvature dipole and valley magnetization in monolayer MoS_2, Phys. Rev. Lett. **123**, 036806 (2019).
[27] B. T. Zhou, C.-P. Zhang, and K. T. Law, Highly tunable nonlinear Hall effects induced by spin-orbit couplings in strained polar transition-metal dichalcogenides, Phys. Rev. Appl. **13**, 024053 (2020).
[28] H. Rostami and V. Juričić, Probing quantum criticality using nonlinear Hall effect in a metallic Dirac system, Phys. Rev. Res. **2**, 013069 (2020).
[29] D.-F. Shao, S.-H. Zhang, G. Gurung, W. Yang, and E. Y. Tsymbal, Nonlinear anomalous Hall effect for Néel vector detection, Phys. Rev. Lett. **124**, 067203 (2020).
[30] L. Zhao, C. A. Belvin, R. Liang, D. A. Bonn, W. N. Hardy, N. P. Armitage, and D. Hsieh, A global inversion-symmetry-broken phase inside the pseudogap region of $YBa_2Cu_3O_y$, Nat. Phys. **13**, 250 (2017).
[31] K. Das, S. Lahiri, R. B. Atencia, D. Culcer, and A. Agarwal, Intrinsic nonlinear conductivities induced by the quantum metric, Phys. Rev. B **108**, L201405 (2023).
[32] W. J. Jankowski and R.-J. Slager, Quantized integrated shift effect in multigap topological phases, Phys. Rev. Lett. **133**, 186601 (2024).
[33] D. Kaplan, T. Holder, and B. Yan, Unification of nonlinear anomalous Hall effect and nonreciprocal magnetoresistance in metals by the quantum geometry, Phys. Rev. Lett. **132**, 026301 (2024).
[34] W. J. Jankowski, A. S. Morris, A. Bouhon, F. N. Ünal, and R.-J. Slager, Optical manifestations and bounds of topological Euler class, Phys. Rev. B **111**, L081103 (2025).
[35] T. Xi, H. Jiang, J. Li, Y. He, Y. Gu, C. Fox, L. Primeau, Y. Mao, J. Rollins, T. Taniguchi, K. Watanabe, D. van der Weide, D. Rhodes, Y. Zhang, Y. Wang, and J. Xiao, Terahertz sensing based on the nonlinear electrodynamics of the two-dimensional correlated topological semimetal $TaIrTe_4$, Nat. Electron. **8**, 578 (2025).
[36] J. Duan, Y. Jian, Y. Gao, H. Peng, J. Zhong, Q. Feng, J. Mao, and Y. Yao, Giant second-order nonlinear Hall effect in twisted bilayer graphene, Phys. Rev. Lett. **129**, 186801 (2022).
[37] N. Wang, D. Kaplan, Z. Zhang, T. Holder, N. Cao, A. Wang, X. Zhou, F. Zhou, Z. Jiang, C. Zhang, S. Ru, H. Cai, K. Watanabe, T. Taniguchi, B. Yan, and W. Gao, Quantum-metric-induced nonlinear transport in a topological antiferromagnet, Nature (London) **621**, 487 (2023).
[38] E. Mönch, M. D. Moldavskaya, L. E. Golub, V. V. Bel'kov, J. Wunderlich, D. Weiss, J. V. Gumenjuk-Sichevska, C. Niu, P. D. Ye, and S. D. Ganichev, Terahertz radiation driven nonlinear transport phenomena in two-dimensional tellurene, Nano Lett. **25**, 476 (2025).
[39] A. Bharti, M. S. Mrudul, and G. Dixit, High-harmonic spectroscopy of light-driven nonlinear anisotropic anomalous Hall effect in a Weyl semimetal, Phys. Rev. B **105**, 155140 (2022).
[40] P. Törmä, S. Peotta, and B. A. Bernevig, Superconductivity, superfluidity and quantum geometry in twisted multilayer systems, Nat. Rev. Phys. **4**, 528 (2022).
[41] Z. Liu and E. J. Bergholtz, Recent developments in fractional Chern insulators, in *Encyclopedia of Condensed Matter Physics*, edited by T. Chakraborty, 2nd ed. (Academic Press, Oxford, UK, 2024), pp. 515–538.
[42] C. Guo, L. Hu, C. Putzke, J. Diaz, X. Huang, K. Manna, F.-R. Fan, C. Shekhar, Y. Sun, C. Felser, C. Liu, B. A. Bernevig, and P. J. W. Moll, Quasi-symmetry-protected topology in a semimetal, Nat. Phys. **18**, 813 (2022).
[43] M. A. Wilde and C. Pfleiderer, Large curvature near a small gap, Nat. Phys. **18**, 731 (2022).
[44] N. Huber, K. Alpin, G. L. Causer, L. Worch, A. Bauer, G. Benka, M. M. Hirschmann, A. P. Schnyder, C. Pfleiderer, and M. A. Wilde, Network of topological nodal planes, multifold degeneracies, and Weyl points in CoSi, Phys. Rev. Lett. **129**, 026401 (2022).
[45] C. Zhong, Y. Chen, Y. Xie, S. A. Yang, M. L. Cohen, and S. Zhang, Towards three-dimensional Weyl-surface semimetals in graphene networks, Nanoscale **8**, 7232 (2016).
[46] Q.-F. Liang, J. Zhou, R. Yu, Z. Wang, and H. Weng, Node-surface and node-line fermions from nonsymmorphic lattice symmetries, Phys. Rev. B **93**, 085427 (2016).
[47] M. A. Wilde, M. Dodenhöft, A. Niedermayr, A. Bauer, M. M. Hirschmann, K. Alpin, A. P. Schnyder, and C. Pfleiderer, Symmetry-enforced topological nodal planes at the Fermi surface of a chiral magnet, Nature (London) **594**, 374 (2021).
[48] J. Ahn, G.-Y. Guo, N. Nagaosa, and A. Vishwanath, Riemannian geometry of resonant optical responses, Nat. Phys. **18**, 290 (2022).
[49] A. Bouhon, A. Timmel, and R.-J. Slager, Quantum geometry beyond projective single bands, arXiv:2303.02180.
[50] W. J. Jankowski, A. S. Morris, Z. Davoyan, A. Bouhon, F. N. Ünal, and R.-J. Slager, Non-Abelian Hopf-Euler insulators, Phys. Rev. B **110**, 075135 (2024).
[51] J. Mitscherling, A. Avdoshkin, and J. E. Moore, Gauge-invariant projector calculus for quantum state geometry and applications to observables in crystals, Phys. Rev. B **112**, 085104 (2025).
[52] P. Fontana, V. Velasco, C. Niu, P. D. Ye, P. V. Lopes, K. E. M. de Souza, M. V. O. Moutinho, C. Lewenkopf, and M. B. S. Neto, Quantum geometry and the electric magnetochiral anisotropy in noncentrosymmetric polar media, Phys. Rev. Lett. **135**, 106602 (2025).
[53] I. Sodemann and L. Fu, Quantum nonlinear Hall effect induced by Berry curvature dipole in time-reversal invariant materials, Phys. Rev. Lett. **115**, 216806 (2015).

[54] Y. Gao, S. A. Yang, and Q. Niu, Field induced positional shift of Bloch electrons and its dynamical implications, Phys. Rev. Lett. **112**, 166601 (2014).

[55] J. Jia, L. Xiang, Z. Qiao, and J. Wang, Equivalence of semiclassical and response theories for second-order nonlinear AC Hall effects, Phys. Rev. B **110**, 245406 (2024).

[56] A. Gao, Y.-F. Liu, J.-X. Qiu, B. Ghosh, T. V. Trevisan, Y. Onishi, C. Hu, T. Qian, H.-J. Tien, S.-W. Chen, M. Huang, D. Bérubé, H. Li, C. Tzschaschel, T. Dinh, Z. Sun, S.-C. Ho, S.-W. Lien, B. Singh, K. Watanabe, *et al.*, Quantum metric nonlinear Hall effect in a topological antiferromagnetic heterostructure, Science **381**, 181 (2023).

[57] M. G. Lopez, D. Vanderbilt, T. Thonhauser, and I. Souza, Wannier-based calculation of the orbital magnetization in crystals, Phys. Rev. B **85**, 014435 (2012).

[58] O. Pozo and F. de Juan, Computing observables without eigenstates: Applications to Bloch Hamiltonians, Phys. Rev. B **102**, 115138 (2020).

[59] A. Graf and F. Piéchon, Berry curvature and quantum metric in N-band systems: An eigenprojector approach, Phys. Rev. B **104**, 085114 (2021).

[60] B. Mera and J. Mitscherling, Nontrivial quantum geometry of degenerate flat bands, Phys. Rev. B **106**, 165133 (2022).

[61] A. Avdoshkin and F. K. Popov, Extrinsic geometry of quantum states, Phys. Rev. B **107**, 245136 (2023).

[62] O. Antebi, J. Mitscherling, and T. Holder, Drude weight of an interacting flat-band metal, Phys. Rev. B **110**, L241111 (2024).

[63] A. Avdoshkin, Geometry of degenerate quantum states, configurations of m-planes and invariants on complex Grassmannians, arXiv:2404.03234.

[64] X.-B. Qiang, T. Liu, Z.-X. Gao, H.-Z. Lu, and X. C. Xie, A clarification on quantum-metric-induced nonlinear transport, Adv. Sci. **13**, e14818 (2026).

[65] H. Isobe, S.-Y. Xu, and L. Fu, High-frequency rectification via chiral Bloch electrons, Sci. Adv. **6**, eaay2497 (2020).

[66] Y. Zhang and L. Fu, Terahertz detection based on nonlinear Hall effect without magnetic field, Proc. Natl. Acad. Sci. U.S.A. **118**, e2100736118 (2021).

[67] J. Wang, H. Zeng, W. Duan, and H. Huang, Intrinsic nonlinear Hall detection of the N'eel vector for two-dimensional antiferromagnetic spintronics, Phys. Rev. Lett. **131**, 056401 (2023).

[68] See Supplemental Material at http://link.aps.org/supplemental/10.1103/4z8z-4kch for details on Eq. (2) and a discussion on how scattering was modeled, the derivation of Eq. (4), a (magnetic) symmetry analysis of the different geometric contributions to the NLHE accompanied by corresponding material candidates, details on the model calculations presented in the main text as well as two further examples, and the derivation of an alternative expression of the NLHE that is suitable for numerical calculations, which includes Refs. [97–129].

[69] Z. Z. Du, C. M. Wang, H.-P. Sun, H.-Z. Lu, and X. C. Xie, Quantum theory of the nonlinear Hall effect, Nat. Commun. **12**, 5038 (2025).

[70] Y. Michishita and R. Peters, Effects of renormalization and non-Hermiticity on nonlinear responses in strongly correlated electron systems, Phys. Rev. B **103**, 195133 (2021).

[71] A. Eberlein, W. Metzner, S. Sachdev, and H. Yamase, Fermi surface reconstruction and drop in the Hall number due to spiral antiferromagnetism in High-T_c cuprates, Phys. Rev. Lett. **117**, 187001 (2016).

[72] S. Verret, O. Simard, M. Charlebois, D. Sénéchal, and A.-M. S. Tremblay, Phenomenological theories of the low-temperature pseudogap: Hall number, specific heat, and Seebeck coefficient, Phys. Rev. B **96**, 125139 (2017).

[73] H. Kontani, T. Tanaka, and K. Yamada, Intrinsic anomalous Hall effect in ferromagnetic metals studied by the multi-d-orbital tight-binding model, Phys. Rev. B **75**, 184416 (2007).

[74] T. Tanaka, H. Kontani, M. Naito, T. Naito, D. S. Hirashima, K. Yamada, and J. Inoue, Intrinsic spin Hall effect and orbital Hall effect in 4d and 5d transition metals, Phys. Rev. B **77**, 165117 (2008).

[75] J. Mitscherling, Longitudinal and anomalous Hall conductivity of a general two-band model, Phys. Rev. B **102**, 165151 (2020).

[76] Y. Michishita and N. Nagaosa, Dissipation and geometry in nonlinear quantum transports of multiband electronic systems, Phys. Rev. B **106**, 125114 (2022).

[77] G. Rickayzen, *Green's Functions and Condensed Matter*, Techniques of Physics No. 5 (Academic Press, London, 1980).

[78] A. Altland and B. D. Simons, *Condensed Matter Field Theory*, 2nd ed. (Cambridge University Press, Cambridge, UK, 2010).

[79] D. E. Parker, T. Morimoto, J. Orenstein, and J. E. Moore, Diagrammatic approach to nonlinear optical response with application to Weyl semimetals, Phys. Rev. B **99**, 045121 (2019).

[80] D. Kaplan, T. Holder, and B. Yan, Unifying semiclassics and quantum perturbation theory at nonlinear order, SciPost Phys. **14**, 082 (2023).

[81] T. Park, X. Huang, L. Savary, and L. Balents, Quantum geometry from the Moyal product: Quantum kinetic equation and nonlinear response, Phys. Rev. B **113**, 045146 (2026).

[82] M. Mehraeen, Quantum kinetic theory of quadratic responses, Phys. Rev. B **110**, 174423 (2024).

[83] M. Mehraeen, Quantum response theory and momentum-space gravity, Phys. Rev. Lett. **135**, 156302 (2025).

[84] J. Rammer and H. Smith, Quantum field-theoretical methods in transport theory of metals, Rev. Mod. Phys. **58**, 323 (1986).

[85] X. Liu, S. S. Tsirkin, and I. Souza, Covariant derivatives of Berry-type quantities: Application to nonlinear transport, arXiv:2303.10129.

[86] D. V. Chichinadze, N. J. Zhang, J.-X. Lin, E. Morissette, X. Wang, K. Watanabe, T. Taniguchi, O. Vafek, and J. I. A. Li, Observation of giant nonlinear Hall conductivity in Bernal bilayer graphene, arXiv:2411.11156.

[87] H. Zhu, J. Li, X. Chen, Y. Yu, and Q. Liu, Magnetic geometry induced quantum geometry and nonlinear transports, Nat. Commun. **16**, 4882 (2025).

[88] Y. D. Wang, Z. F. Zhang, Z.-G. Zhu, and G. Su, Intrinsic nonlinear Ohmic current, Phys. Rev. B **109**, 085419 (2024).

[89] C. Wang, Y. Gao, and D. Xiao, Intrinsic nonlinear Hall effect in antiferromagnetic tetragonal CuMnAs, Phys. Rev. Lett. **127**, 277201 (2021).

[90] H. Liu, J. Zhao, Y.-X. Huang, W. Wu, X.-L. Sheng, C. Xiao, and S. A. Yang, Intrinsic second-order anomalous Hall effect and its application in compensated antiferromagnets, Phys. Rev. Lett. **127**, 277202 (2021).

[91] P. Tang, Q. Zhou, G. Xu, and S.-C. Zhang, Dirac fermions in an antiferromagnetic semimetal, Nat. Phys. **12**, 1100 (2016).

[92] D. Di Sante, A. Hausoel, P. Barone, J. M. Tomczak, G. Sangiovanni, and R. Thomale, Realizing double Dirac particles in the presence of electronic interactions, Phys. Rev. B **96**, 121106(R) (2017).

[93] Y. Zhang, H. Zeng, and H. Huang, Logarithmically enhanced intrinsic nonlinear Hall effects in $\mathcal{PT}$-symmetric antiferromagnetic nodal-line semimetals, Phys. Rev. B **111**, L081115 (2025).

[94] S. V. Gallego, J. M. Perez-Mato, L. Elcoro, E. S. Tasci, R. M. Hanson, K. Momma, M. I. Aroyo, and G. Madariaga, *MAGNDATA* : Towards a database of magnetic structures. I. The commensurate case, J. Appl. Crystallogr. **49**, 1750 (2016).

[95] S. V. Gallego, J. M. Perez-Mato, L. Elcoro, E. S. Tasci, R. M. Hanson, M. I. Aroyo, and G. Madariaga, *MAGNDATA* : Towards a database of magnetic structures. II. The incommensurate case, J. Appl. Crystallogr. **49**, 1941 (2016).

[96] Z. Guo, X.-Y. Liu, H. Wang, L. kun Shi, and K. Chang, Dissipation-shaped quantum geometry in nonlinear transport, arXiv:2511.16422.

[97] S. S. Tsirkin and I. Souza, On the separation of Hall and Ohmic nonlinear responses, SciPost Phys. Core **5**, 039 (2022).

[98] I. A. Ado, I. A. Dmitriev, P. M. Ostrovsky, and M. Titov, Anomalous Hall effect with massive Dirac fermions, Europhys. Lett. **111**, 37004 (2015).

[99] K. Alpin, M. M. Hirschmann, N. Heinsdorf, A. Leonhardt, W. Y. Yau, X. Wu, and A. P. Schnyder, Fundamental laws of chiral band crossings: Local constraints, global constraints, and topological phase diagrams, Phys. Rev. Res. **5**, 043165 (2023).

[100] T. Bzdušek and M. Sigrist, Robust doubly charged nodal lines and nodal surfaces in centrosymmetric systems, Phys. Rev. B **96**, 155105 (2017).

[101] G. Chang, B. J. Wieder, F. Schindler, D. S. Sanchez, I. Belopolski, S.-M. Huang, B. Singh, D. Wu, T.-R. Chang, T. Neupert, S.-Y. Xu, H. Lin, and M. Z. Hasan, Topological quantum properties of chiral crystals, Nat. Mater. **17**, 978 (2018).

[102] T. Chen, S. Minami, A. Sakai, Y. Wang, Z. Feng, T. Nomoto, M. Hirayama, R. Ishii, T. Koretsune, R. Arita, and S. Nakatsuji, Large anomalous Nernst effect and nodal plane in an iron-based kagome ferromagnet, Sci. Adv. **8**, eabk1480 (2022).

[103] S. A. Chen, R. Moessner, and T. K. Ng, Generalized Peierls substitution for Wannier obstructions: Response to disorder and interactions, Phys. Rev. Lett. **135**, 116502 (2025).

[104] J. Li, Y. Li, S. Du, Z. Wang, B.-L. Gu, S.-C. Zhang, K. He, W. Duan, and Y. Xu, Intrinsic magnetic topological insulators in van der Waals layered $MnBi_2Te_4$-family materials, Sci. Adv. **5**, eaaw5685 (2019).

[105] G. Frank, D. Varjas, G. Pintér, and A. Pályi, Weyl-point teleportation, Phys. Rev. B **109**, 205415 (2024).

[106] B.-B. Fu, C.-J. Yi, T.-T. Zhang, M. Caputo, J.-Z. Ma, X. Gao, B. Q. Lv, L.-Y. Kong, Y.-B. Huang, P. Richard, M. Shi, V. N. Strocov, C. Fang, H.-M. Weng, Y.-G. Shi, T. Qian, and H. Ding, Dirac nodal surfaces and nodal lines in ZrSiS, Sci. Adv. **5**, eaau6459 (2019).

[107] L.-H. Hu, C. Guo, Y. Sun, C. Felser, L. Elcoro, P. J. W. Moll, C.-X. Liu, and B. A. Bernevig, Hierarchy of quasisymmetries and degeneracies in the CoSi family of chiral crystal materials, Phys. Rev. B **107**, 125145 (2023).

[108] K.-E. Huhtinen and P. Törmä, Conductivity in flat bands from the Kubo-Greenwood formula, Phys. Rev. B **108**, 155108 (2023).

[109] H. T. Stokes, D. M. Hatch, and B. J. Campbell, Iso-mag, ISOTROPY software suite, https://iso.byu.edu/.

[110] S.-X. Li, W. Wang, S. Xu, T. Li, Z. Li, J. Wang, J.-J. Mi, Q. Tao, F. Tang, X. Wan, and Z.-A. Xu, Giant anomalous Hall effect in kagome nodal surface semimetal Fe_3Ge, Phys. Rev. B **112**, 184418 (2025).

[111] J.-Z. Ma, Q.-S. Wu, M. Song, S.-N. Zhang, E. B. Guedes, S. A. Ekahana, M. Krivenkov, M. Y. Yao, S.-Y. Gao, W.-H. Fan, T. Qian, H. Ding, N. C. Plumb, M. Radovic, J. H. Dil, Y.-M. Xiong, K. Manna, C. Felser, O. V. Yazyev, and M. Shi, Observation of a singular Weyl point surrounded by charged nodal walls in PtGa, Nat. Commun. **12**, 3994 (2021).

[112] Wolfram Inc., Mathematica, Version 14.0, https://www.wolfram.com/mathematica/.

[113] J. Mitscherling, Electrical conductivity in quantum materials, Ph.D. thesis, Universität Stuttgart, 2021.

[114] J. Mitscherling and T. Holder, Bound on resistivity in flat-band materials due to the quantum metric, Phys. Rev. B **105**, 085154 (2022).

[115] J. Mitscherling, D. S. Borgnia, S. Ahuja, J. E. Moore, and V. B. Bulchandani, Orbital Wigner functions and quantum transport in multiband systems, arXiv:2502.14026.

[116] R. Oiwa and H. Kusunose, Systematic analysis method for nonlinear response tensors, J. Phys. Soc. Jpn. **91**, 014701 (2022).

[117] D. Varjas, F. de Juan, and Y.-M. Lu, Bulk invariants and topological response in insulators and superconductors with nonsymmorphic symmetries, Phys. Rev. B **92**, 195116 (2015).

[118] D. J. Thouless, M. Kohmoto, M. P. Nightingale, and M. den Nijs, Quantized Hall conductance in a two-dimensional periodic potential, Phys. Rev. Lett. **49**, 405 (1982).

[119] A. Rich, P. Scheibe, and N. Abbasi, Rule-based integration: An extensive system of symbolic integration rules, J. Open Source Softw. **3**, 1073 (2018).

[120] A. Scheie, P. Laurell, P. A. McClarty, G. E. Granroth, M. B. Stone, R. Moessner, and S. E. Nagler, Dirac magnons, nodal lines, and nodal plane in elemental gadolinium, Phys. Rev. Lett. **128**, 097201 (2022).

[121] F. Tang and X. Wan, Complete classification of band nodal structures and massless excitations, Phys. Rev. B **105**, 155156 (2022).

[122] O. Türker and S. Moroz, Weyl nodal surfaces, Phys. Rev. B **97**, 075120 (2018).

[123] D. Vanderbilt, *Berry Phases in Electronic Structure Theory: Electric Polarization, Orbital Magnetization and Topological Insulators* (Cambridge University Press, Cambridge, UK, 2018).

[124] W. Wu, Y. Liu, S. Li, C. Zhong, Z.-M. Yu, X.-L. Sheng, Y. X. Zhao, and S. A. Yang, Nodal surface semimetals: Theory and material realization, Phys. Rev. B **97**, 115125 (2018).

[125] M. Xiao, L. Ye, C. Qiu, H. He, Z. Liu, and S. Fan, Experimental demonstration of acoustic semimetal with topologically charged nodal surface, Sci. Adv. **6**, eaav2360 (2020).

[126] C. Xie, H. Yuan, Y. Liu, X. Wang, and G. Zhang, Three-nodal surface phonons in solid-state materials: Theory and material realization, Phys. Rev. B **104**, 134303 (2021).

[127] R. Yamada, M. T. Birch, P. R. Baral, S. Okumura, R. Nakano, S. Gao, M. Ezawa, T. Nomoto, J. Masell, Y. Ishihara, *et al.*, A metallic *p*-wave magnet with commensurate spin helix, Nature (London) **646**, 837 (2025).

[128] Z.-M. Yu, W. Wu, Y. X. Zhao, and S. A. Yang, Circumventing the no-go theorem: A single Weyl point without surface Fermi arcs, Phys. Rev. B **100**, 041118(R) (2019).

[129] X. Zhang, Z.-M. Yu, Z. Zhu, W. Wu, S.-S. Wang, X.-L. Sheng, and S. A. Yang, Nodal loop and nodal surface states in the Ti_3Al family of materials, Phys. Rev. B **97**, 235150 (2018).